Wind-Mixed Layer Deepening Scaling Law in a Rotating Frame

M. Coppin[1,2], B. Deremble,[1], J. Sommeria[2]

[1]IGE, CNRS UMR5001, Grenoble, France
[2]LEGI, CNRS UMR5519, Grenoble, France

Key Points:

- We propose a theory for a scaling law of the deepening of the mixed layer induced by the wind forcing which considers the earth's rotation

Corresponding author: Max Coppin, max.coppin@univ-grenoble-alpes.fr

Abstract

The deepening of the mixed layer (ML) is a phenomenon forced by wind stress or heat flux. Scaling laws exist to predict its evolution but they either do not take into account the Earth's rotation or do not explain the turbulent mixing mechanisms involved. Here, we study the deepening of the wind-mixed layer in a linearly stratified and rotating ocean. We describe the turbulent mixing processes in an analytical framework using the $k-\epsilon$ model. We show that mixing is mainly confined to a marginally stable entrainment layer at the bottom of the ML. We propose a scaling law for the time dependence of the deepening rate of the ML $h \sim t^{1/5}$ as a function of the mixing efficiency the potential energy conversion and the dissipation profile.

Keyword: Mixed-layer depth, Mixing-efficiency, TKE, Turbulent convection, Sear-driven turbulence

Plain Language Summary

Understanding the deepening of the mixed layer in the ocean is key to predicting climate and ocean circulation. This process, driven by wind and heat flux, has an impact on the exchange of heat, nutrients and carbon between the ocean surface and deeper ocean. In our study, we investigate how wind-induced mixing affects the depth of the mixed layer in a rotating and stratified ocean. By developing a new scaling law describing the rate at which the mixed layer deepens over time, we gain insight into the complex interactions between turbulent mixing processes and ocean dynamics. This research is leading to a better understanding of the role of the ocean in regulating climate.

1 Introduction

The Mixed layer (ML) deepening is characterised by turbulent convective mixing caused by mechanical stress (momentum flux) or by a buoyancy flux. Its dynamics is also affected by the Earth's rotation. The coriolis parameter plays a stabilising role by reducing turbulent convection mixing (Jones and Marshall (1993); Sander et al. (1995); Mironov et al. (2000)), reducing convective instability (Veronis (1959); Chandrasekhar (1997); Carpenter et al. (2022)) and reducing its velocity (Fernando et al. (1991)).

Pollard et al. (1973) (hereafter P73) studied the evolution of the mixing layer (ML) and formalized a scaling law for its thickness h for a constant surface stress τ with no heat fluxes and linear stratification N. It is a separated expression for time prior and beyond half the inertial time scale $T_f = 2\pi/f$

$$h(t) = (u_*)^{1/2}\left[\frac{4(1-\cos(ft))}{f^2N^2}\right]^{1/4} \quad t < \frac{T_f}{2} \tag{1}$$

$$= 1.7\left(\frac{u_*}{\sqrt{Nf}}\right) \quad t > \frac{T_f}{2} \tag{2}$$

with $u_* = \sqrt{\frac{\tau}{\rho}}$ the friction velocity at the surface and we use the notation

$$L_{P73} = \frac{u_*}{\sqrt{Nf}} \tag{3}$$

as characteristic length from the P73's scaling law.
We also define from the equation (3.1) in the paper of P73 a characteristic velocity of the ML U_{p73}

$$U_{p73} = \frac{u_*^2}{fL_{p73}} = u_*\sqrt{\frac{N}{f}}. \tag{4}$$

This scaling law is used in a large number of models (Zilitinkevich et al. (1979), Lozovatsky et al. (2005)). It is particularly robust with no rotation since at short time,

P73 reduced to the expression verify experimentally by Kato and Phillips (1969)

$$h(t) = u_* \left(\frac{1}{2}\right)^{1/4} \sqrt{\frac{t}{N}} \tag{5}$$

For longer time, P73 proposed that the ML reaches a maximum and no longer deepens. However, it appears that there is a change in the regime after one half of inertial period and the mixing layer continues to deepen (Ushijima and Yoshikawa (2020)) (hereafter U20).

U20 performed a series of LES experiments in which the friction speed u_*, rotation f and stratification N were varied. They showed the dependency of the ML deepening on the Rossby number and the Froude number and propose the time-dependant scaling

$$h = 1.5 L_{p73} \left(\frac{f}{N}\right)^{-2.2\times10^{-2}} \left(\frac{t}{T_f}\right)^{0.18} \tag{6}$$

For a range of parameter f/N between $\left[1.3 \times 10^{-3} \text{ and } 2.0 \times 10^{-4}\right]$. This scaling is based on an optimal adjustment of the parameters from the LES, However U20 does not describe the mechanisms that explain this scaling and their contribution.

In this paper we are interested in the physical process involved in the ML formation after the half of an inertial period. We propose to diagnose the ML deepening mechanism in presence of rotation by using idealised 1D numerical simulations. Then to build a theoretical frame for a scaling law.We begin in section 2 by describing the $k-\epsilon$ turbulent closure model. In section 3 we quantify the energy exchanges in the water column. A diagnostic of mixing and dissipation is given in section 4. In section 5 we formalise the scaling law and explore the limits of the proposed assumption. We conclude in section 6.

2 Model and Methods

2.1 $k-\epsilon$ Model

Consider the x, y-momentum equation in a 1D rotating frame and the buoyancy equation without heat fluxes

$$\frac{\partial \overline{u}}{\partial t} + (\overline{\mathbf{u}} \cdot \nabla)\overline{u} - f\overline{v} = \frac{1}{\rho}\frac{\partial \overline{p}}{\partial x} + \nu\nabla^2\overline{u} - \frac{\partial}{\partial z}\overline{u'w'} \tag{7}$$

$$\frac{\partial \overline{v}}{\partial t} + (\overline{\mathbf{u}} \cdot \nabla)\overline{v} - f\overline{u} = \frac{1}{\rho}\frac{\partial \overline{p}}{\partial y} + \nu\nabla^2\overline{v} - \frac{\partial}{\partial z}\overline{v'w'} \tag{8}$$

$$\frac{\partial \overline{b}}{\partial t} + (\overline{\mathbf{u}} \cdot \nabla)\overline{b} = \frac{\partial}{\partial_z}\left(\nu'\frac{\partial \overline{b}}{\partial_z} - \overline{w'b'}\right) \tag{9}$$

The $k-\epsilon$ model is a turbulent closure of order 2. It closes the Reynolds's average equation by adding two prognostic transport equations, one for the turbulent kinetic energy $k = u'^2 + v'^2$ and the other for the dissipation ϵ.
Neglecting advecting terms.

$$\frac{\partial k}{\partial t} - \frac{\partial}{\partial z}\left(\left(\nu + \frac{\nu_t}{\sigma_k}\right)\frac{\partial k}{\partial_z}\right) = P - B - \epsilon \tag{10}$$

$$\frac{\partial \epsilon}{\partial t} - \frac{\partial}{\partial z}\left(\left(\nu + \frac{\nu_t}{\sigma_\epsilon}\right)\frac{\partial \epsilon}{\partial_z}\right) = \frac{\epsilon}{k}(c_{1\epsilon}P - c_{3\epsilon}B - c_{2\epsilon}\epsilon) \tag{11}$$

Where σ_k the turbulent Schmidt number, $c_{1\epsilon}, c_{2\epsilon}, c_{3\epsilon}$ empirical parameters (Canuto et al. (2001)).
The turbulent fluxes are computed as follows (Rodi (1987)Burchard (2002b))

$$P = -\overline{u'w'}\partial_z\overline{u} = \nu_t(\partial_z\overline{u})^2 \tag{12}$$
$$B = \overline{w'b'} = -\nu'_t(\partial_z b) \tag{13}$$

with $b = -g\dfrac{\Delta\rho}{\rho}$ and the diffusivity ν_t and ν'_t respectively of momentum and heat are parameterised using stability functions c_μ and c'_μ (Canuto et al. (2001); Burchard and Bolding (2001)) such that :

$$\nu_t = c_\mu\frac{k^2}{\epsilon} \qquad \nu_t = c_\mu\frac{k^2}{\epsilon} \tag{14}$$

In this model, the buoyancy production is directly linked to the potential energy (Burchard, 2002a)

$$\frac{\partial E_p}{\partial t} = \int_{-H}^{0}\nu'_t\frac{\partial b}{\partial z}dz = \int_{-H}^{0} -Bdz. \tag{15}$$

Here the capital E_p refer to the integrated potential energy $e_p = -zb$.

This model has been shown to be robust in convective processes (Burchard and Bolding (2001); Umlauf et al. (2003)) since it correctly reproduces the basic interaction mechanisms between shear, stratification and turbulence. A review of turbulence closure models, and in particular the $k-\epsilon$ model, is presented in (Burchard, 2002a).

2.2 Numerical Model

We use the open-source numerical model GOTM (General Ocean Turbulence Model) *https://gotm.net/*. This Model solves the momentum, salt and heat transport equations over a 1D water column. All horizontal gradients are either parameterised, neglected, or obtained prognostically where possible. Our configuration solves equation (11) for a Coriolis parameter $f \in [5.910^{-5}; 1.0210^{-4}]$ s^{-1}, a stratification $N^2 \in [2.510^{-5}; 210^{-3}]$ s^{-1} (same range of parameter f/N as U20). A velocity friction $u_* = 1.10^{-2}$ ms^{-1}, a simulation span of 10 days for a time step of 60 s. The vertical resolution is 50 cm for a domain of 500 m in the z-axis.

Figure 6 show the evolution of h in time using this model, we observe an evolution law $h(t) \sim t^{1/5}$ which is close the power found by U20 $h_{U20}(t) \sim t^{0.18}$. This numerical model is in good agreement with U20. Therefore GOTM and thus the $k-\epsilon$ model are adapted to the modelling of the turbulent convection. and represent this process with a reliability which is near of the one offered by LES.

3 Energetic of the Mixed Layer Deepening

We examine the analytically the evolution of the potential energy associated with the depth of the mixing layer. We analyse how this potential energy is affected by changes in the density profile, and identify a structure for the water column based on vertical density and velocity profiles.

3.1 Potential Energy Evolution

The initial density profile is given by

$$\rho_i(z) = \rho_0(1 - \frac{N^2}{g}z) \tag{16}$$

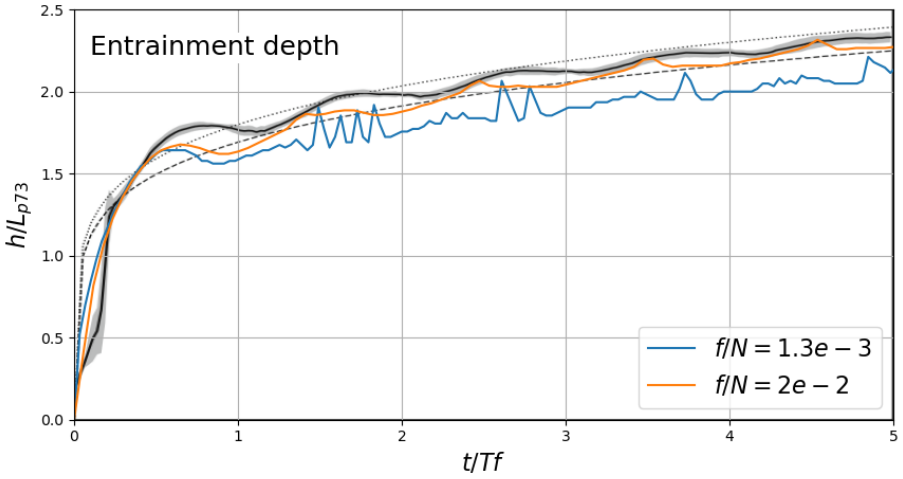

Figure 1. Temporal variation of the MLD normalizes by L_{p73} the color curves are plotted on the Fig 3a) of U20. The solid dark line is the averaged value of all the U20 experiment. The Dashed and doted lines are the estimation of the (Eq 6) with the greatest ($f/N = 2.0 \times 10^{-2}$) and smallest ($f/N = 1.3 \times 10^{-3}$) f/N parameter range of the U20's study. The colors lines are GOTM simulation for the two different f/N parameter.

The density of the ML is

$$\rho_m = \frac{\rho_i(z=0) + \rho_i(z=-h)}{2} = \rho_0(1 - \frac{N^2}{2g}h). \tag{17}$$

As h deepens, the density ρ_m of the mixing layer increases because it has been mixed with the denser water below. Therefore, over time, the centre of mass is shifted upward. Considering a vertical density profile of a water column composed by a mixed layer and a stratified one, we can write the expression of the specific potential energy.

$$E_p = \frac{1}{\rho_0}\int_{-H}^{0} \rho g z dz \tag{18}$$

We plug in the density profile of the ML (eq. 17) and the lower part at rest (eq. 16)

$$E_p = \left(-\frac{gH^2}{2} - \frac{N^2H^3}{3} + \frac{1}{12}N^2h^3\right) \tag{19}$$

The first two terms correspond to the initial potential energy and the last term represent the gain due to the lift of the centre of mass.
Taking the derivative of this equation gives the time evolution of the potential energy, which is positive. Thus, a deepening of the ML correspond to gain of potential energy.

$$\frac{dEp}{dt} = \frac{N^2}{12}\frac{dh^3}{dt} \tag{20}$$

The Fig (2) show the structure of the water column. From the top to the bottom, three layers can be defined.

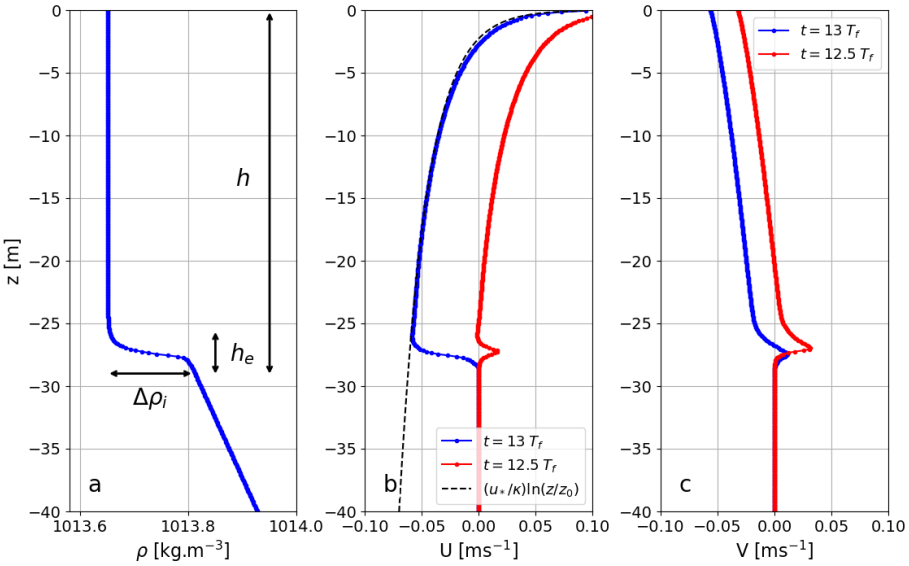

Figure 2. Vertical profile of (a) density, (b) along-wind velocity U and (c) cross-wind velocity V. In blue, the last inertial period $t = 13\ T_f$. In red the last half inertial period $t = 12.5\ T_f$. In black the logarithmic profile of the velocity from the "Law of the wall" $\frac{u_*}{\kappa}\ln(\frac{z}{z_0})$. The parameters of the simulation are : $f = 10^{-4}$ s^{-1}, $N^2 = 10^{-4}$ s^{-1} and the wind stress $\tau = 0.1027$ m^2 s^{-2}

- A well mixed layer $z \in [0, -h + h_e]$ in which the density is uniform. The along-wind velocity follow a logarithmic profile

$$\frac{\partial \overline{u}}{\partial z} = \frac{u_*}{\kappa z} \tag{21}$$

with κ the Von Karman constant. This expression come from the *law of the wall* due to the frictional behaviour of the wind stress. This velocity profile is expected due to the $k - \epsilon$ model implementation.
- An entrainment layer $z \in [-h+h_e, -h]$. This layer forms the transition between the other two layers. It contains on the thickness h_e, the density jump $\Delta\rho = N^2 h$ and the velocity jump ΔU.
- A lower part with $z \in [-h, -H]$. This layer is not affected by the surface shear and is therefore at rest with the background stratification

3.2 Local Turbulent Kinetic Energy Balance

The input of energy at the top of the water column is converted into turbulent Shear, which is transported in the water column by turbulent processes. The evolution of the MLD can be retrieved by the buoyancy production. We thus need to consider the turbulent kinetic energy (k) equation (11).

At first, as the near sub surface velocity increase, accelerating the mixed layer. After half of the inertial period we see in Fig 3 (Top) that the velocity drops due to the onset of an inertial oscillation. As a result the layer reaches a periodic equilibrium. However there is still an injection of energy at the surface and the mixing layer continues to deepen as the fig **??** shows but does not accelerate. As a result we observe TKE reaching steady as shown Fig (3) (Bottom)

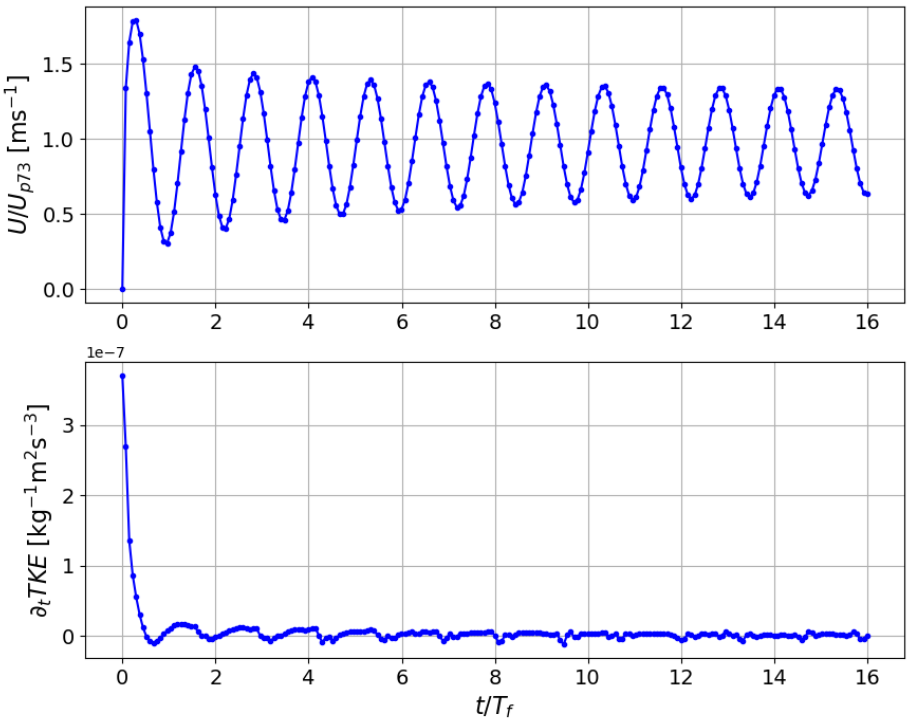

Figure 3. Time evolution of the time derivative of the surface along-wind velocity (Top) and TKE integrated over the water column (Bottom). $f = 10^{-4}$ s^{-1}, $N^2 = 10^{-4}$ s^{-1} and the wind stress $\tau = 0.1027$ m^2 s^{-2}

Thus there is a balance between the terms on the right hand sides. Hence

$$P - B = \epsilon. \tag{22}$$

We can use the expression of the Richardson flux $Ri_f = \dfrac{-B}{P}$ in the equation (22)

$$1 + \frac{P}{B} = -\frac{\epsilon}{B} \tag{23}$$

$$-B = \frac{Ri_f}{1 + Ri_f}\epsilon \tag{24}$$

$$-B = \Gamma\epsilon \tag{25}$$

With the mixing efficiency $\Gamma = \dfrac{Ri_f}{1 + Ri_f}$ defined empirically ((Osborn, 1980)) with a value of $\Gamma_{t0} = 0.2$. Fig 4 represent its vertical profile. From it we can approximate the vertical profile of Gamma as being a piecewise constant function null everywhere except in the entrainment layer and with a value of $\Gamma_0 = 0.25$. Note that below the entrainment layer, Gamma tends towards 1 for reasons of numerical stability (B takes a threshold value and P is null). The mixing efficiency is zero in this region of the water column. From now we will use the approximated function instead of the real profile. We call it Γ for more simplicity.

This equation is a relationship between the production of buoyancy, dissipation and mixing efficiency.
Although we consider a ML, nothing suggests that the mixing process is uniform in this layer. The subject of the next section is, therefore, the nature of the mixing and dissipation and their vertical distribution.

4 Mixing and Dissipation law

4.1 Interface Mixed/Stratified layer

We have seen above with the density and velocity profiles that the water column has a vertical structure which consists of three distinct layers. Let's perform a heuristic diagnostic to measure the thickness of the entrainment layer by describing the vertical structure of the mixture.
In the upper layer, the velocity has a logarithmic profile and, since the layer is already mixed and therefore uniform (fig 2 a)) , we can assume there is very little mixing.
In contrast, the entrainment layer contains a very high density jump and a very high velocity shear on the thickness h_e. It is therefore in this layer that the mixing is greatest. This mixing is caused by a velocity shear which is all the greater the thinner its thickness. This layer is therefore marginally stable.
Then the bottom layer is not affected by the surface shear and is therefore at rest with the background stratification and so zero mixing.

$$Ri = \frac{g\frac{\partial \rho}{\partial z}}{(\frac{\partial U}{\partial z})^2} = Ri_c \tag{26}$$

with the density leap: $\dfrac{\partial \rho}{\partial z} = \dfrac{\Delta \rho_i}{h_e} = \dfrac{N^2 h}{h_e}$

We observe in Fig (3 (b)), that the velocity in the ML follow a logarithmic profile

$$\frac{\partial \overline{u}}{\partial z} = \frac{u_*}{\kappa z} \tag{27}$$

with κ the Von Karman constant. This expression come from the *law of the wall* due to the frictional behaviour of the wind stress. We also see that the velocity profile is oscillating between a peak and a trough of the inertial period. As a result, the shear at the bottom of the mixing layer varies within an inertial period. The first consequence of this is that we need to estimate an average value for this shear between $-h + h_e$ and $-h$. We use the characteristic velocity U_{p73} (4). Furthermore, in order to obtain a power law, we need to discard a logarithmic correction. We therefore obtain an expression for the velocity shear between the mixed layer and the stratified layer at rest

$$\frac{\partial U}{\partial z} = \frac{u(-h + h_e) - 0}{h_e} = \frac{u_* \sqrt{\frac{N}{f}}}{h_e}. \tag{28}$$

The second consequence is that the marginal stability condition is also periodic since it is only valid for a sufficiently large shear. The precise evaluation of the Richardson number under these conditions is complex, so we will adopt a bulk formulation in the entrainment layer with $Ri_c = O(1)$. This formulation is commonly used in ML deepening models (Pollard et al. (1973); Price et al. (1986)).

Hence, we obtain a relation for the entrainment layer thickness

$$h_e = Ri_c \frac{u_*^2}{Nf} \frac{1}{h} \tag{29}$$

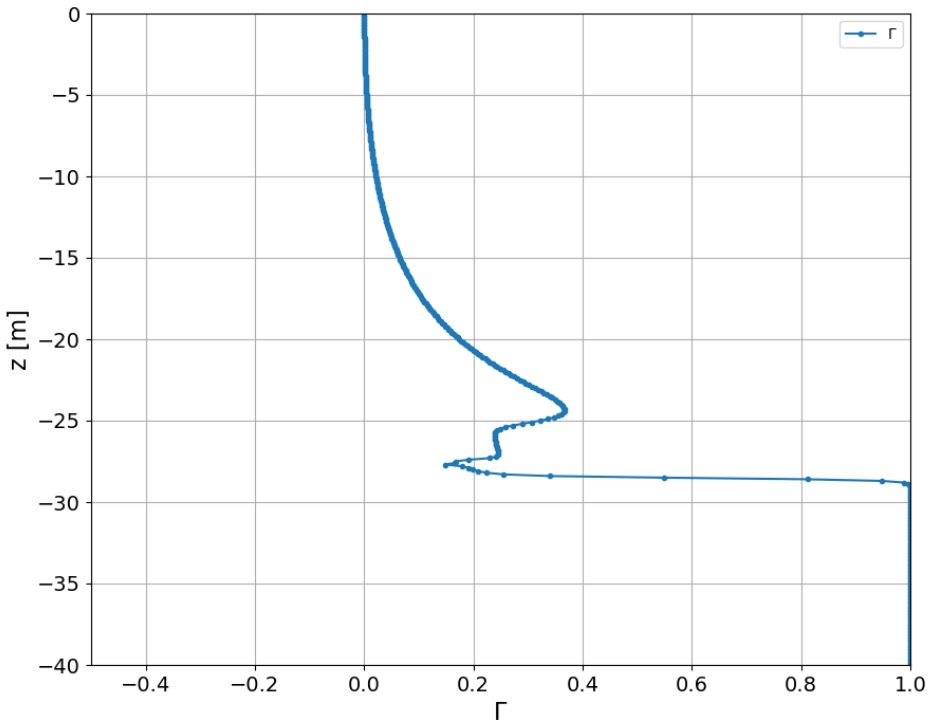

Figure 4. Vertical profile of the mixing efficiency at the last moment of the simulation. The bold line is the profile obtained by the simulationsImplicitly, the contour of the function delimits the three parts: from top to bottom: the Mixed layer, the entrainment layer and the bottom layer. $f = 10^{-4}$ s^{-1}, $N^2 = 10^{-4}$ s^{-1} and the wind stress $\tau = 0.1027$ m^2 s^{-2}. Bellow the mixed layer the shear stress is null and thus the Γ tend to 1.

4.2 Mixing efficiency

The integral of the combination of the eq (15) and (25) can be decomposed on the three intervals describe above. Due to the zero value of the mixing efficiency in the mixing layer and the deep layer, we can therefore write

$$\frac{\partial E_p}{\partial t} = \int_{-h}^{-h+h_e} \Gamma \epsilon dz \simeq \Gamma_0 h_e \epsilon(z = -h) \tag{30}$$

Thus

$$\frac{\partial E_{pot}}{\partial t} = Ri_c \Gamma_0 \frac{u_*^2}{Nf} \frac{1}{h} \epsilon(z = -h). \tag{31}$$

4.3 Dissipation Vertical Profile

To determine the nature of the vertical profile of the ϵ dissipation we consider the TKE balance equation. At the surface we have $B = 0$.
And as our system is quasi-stationary we have that $\dfrac{\partial k}{\partial t} = 0$.
Hence, near the surface

$$\epsilon = -P.$$

The vertical profile of the dissipation is assumed by interpolating its surface expression throughout the mixed layer. Using the logarithmic profile of the velocity (Fig 27) and using the constant flux approximation $u'w' = u_*^2$

$$\epsilon(z) = \frac{u_*^3}{\kappa z} \tag{32}$$

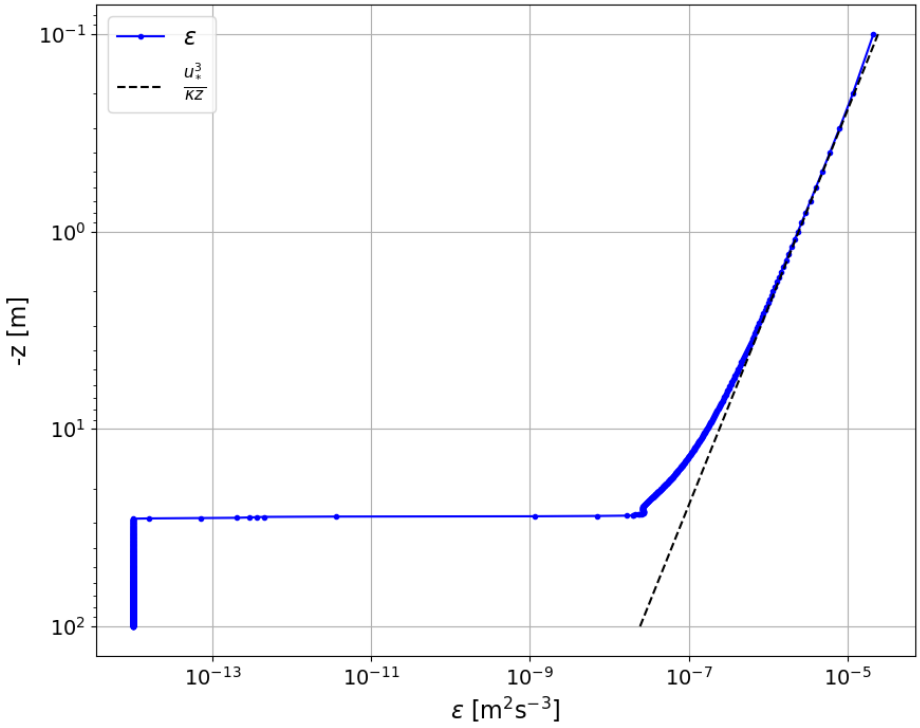

Figure 5. Vertical profile of the dissipation ϵ (blue solid line) the last instant of the simulation. And a law $1/z$ (dashed line). T. $f = 10^{-4}$ s^{-1}, $N^2 = 10^{-4}$ s^{-1} and the wind stress $\tau = 0.1027$ m^2 s^{-2}

The approximation we made by interpolating the surface dissipation expression over the entire ML is consistent, since we observe in Fig (5) the same order of magnitude at the top of the entrainment layer, (above the leap).

Using the equations (20),(31)

$$\frac{N^2}{12}\frac{\partial h^3}{\partial t} = Ri_c\Gamma_0\frac{u_*^2}{Nf}\frac{1}{h}\epsilon(z=-h) \tag{33}$$

and by replacing the expressions of the dissipation at the depth h using 32

$$\frac{\partial h^5}{\partial t} = \left(20Ri_c\Gamma_0\frac{u_*^5}{N^3 f\kappa}\right) \tag{34}$$

and by time integration

$$h(t) = \left(20Ri_c\Gamma_0\frac{u_*^5}{N^3 f\kappa}\right)^{1/5} t^{1/5}. \tag{35}$$

We write this equation using the same formulation as Ushijima and Yoshikawa (2020)

$$h(t) = L_{p73}\left(40\pi Ri_c\frac{\Gamma_0}{\kappa}\right)^{1/5}\left(\frac{f}{N}\right)^{\frac{1}{10}}\left(\frac{t}{T_f}\right)^{1/5} \tag{36}$$

We therefore obtain a law that predicts deepening at a rate $t^{1/5}$. This rate is consistent with the one computed by U20. We also note that the coefficient $\frac{f}{N}$ is quite different from the value of U20 but remain very small and the the sensibility of the scaling law within the range of the ($\frac{f}{N}$) values set by U20 ($\frac{f}{N} = 1.3 \times 10^{-3}$ for the smallest and $\frac{f}{N} = 2.0 \times 10^{-4}$ for the greatest) is negligible.

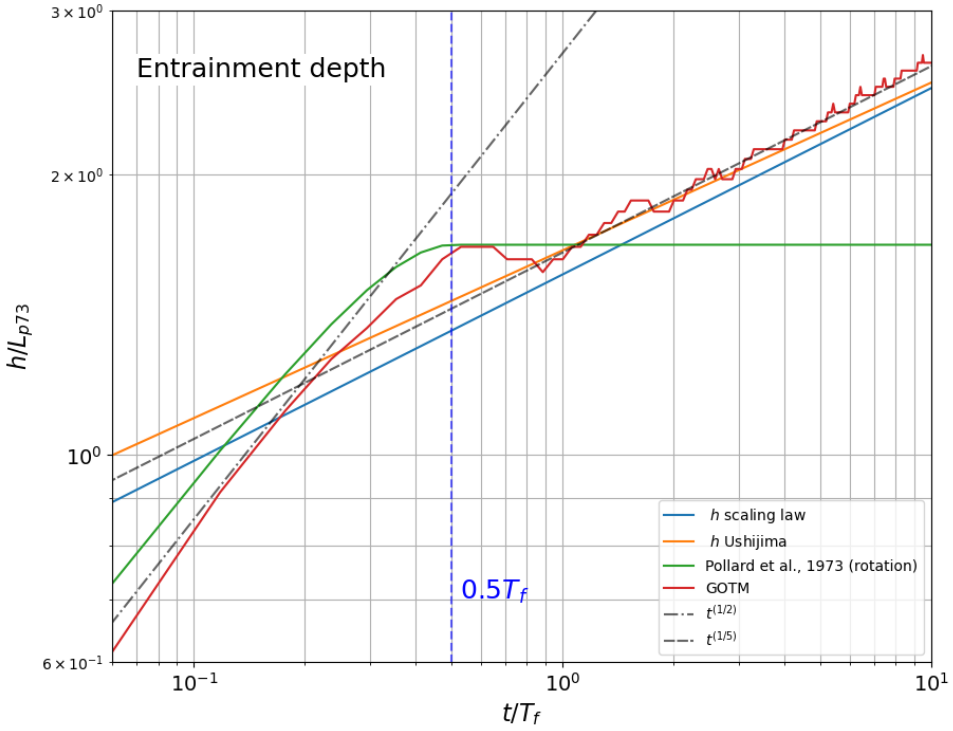

Figure 6. Time evolution of the mixed layer depth (MLD) in solid lines simulated by the numerical model (red), the scaling law predicted by Pollard et al, (green), the scaling law found by U20 (in orange) and the analytical scaling law demonstrated in this paper (in light blue) . Dark dashed line are the temporal evolution power 1/2 and 1/5. The vertical dashed blue line indicates half of the inertial period $0.5T_f$. The Coriolis parameter for the analytical law and the simulation is $f = 10^{-4}$ s^{-1}, $N^2 = 10^{-4}$ s^{-1} and the wind stress $\tau = 0.1027$ m^2 s^{-2}

We can compare in Fig 6 the value of our scaling to the value obtain with the scaling of U20 and the numerical simulation. We observe our scaling underestimate the ML deepening. However, because the time dependency is greater in our formulation that the U20 one. The relative error of our MLD estimate to U20 $\frac{h_{U20} - h}{h_{U20}}$ reduce from 4.5 % to 2 T_f to 1 % to 12 T_f. We can therefore conclude to the constancy of our scaling law and show the validity of our theoretical framework.

4.4 Limitations

We have considered each of these to be valid as long as they respect the same order of magnitude as the simulated values. We summarise them here:
- We wanted an analytical solution in the form of a power law of the deepening rate of the ML. Thus we had to consider the stratification to be linear and apply logarithmic corrections to the velocity at the base of the entrainment layer.
- We approximated the mixing efficiency profile to be non-null only in the entrainment layer. In reality, mixing is still occurring in the upper part of the ML since its density increases as the layer thickens, as shown by its expression eq (17). In the deep layer bellow the ML, internal waves are generated by the deepening of the ML, creating some mixing.
- We interpolated the dissipation profile from a valid surface expression.
- We have used the expression of a critical Richardson number to define the thickness of the entrainment layer. This approach is more refined than a Bulk Richardson number over the entire ML (Pollard et al. (1973); Price et al. (1986)). Yet, due to inertial oscillations, this layer is in a marginal stability state only when the shear at the base of the ML is maximal. The GOTM model is a faithful representation of the turbulent convection phenomenon, but it appears that for small f/N, the ML deepening is undervalued. Hence the dependence of the f/N factor is much greater in our scaling ($\left(\frac{f}{N}\right)^{1/10}$) than in that of U20 ($\left(\frac{f}{N}\right)^{-2.2\times10^{-2}}$).

5 Concluding Remarks

In this study we have developed a theoretical framework to explain the deepening of the ML in the case of an ocean forced by surface stress without heat loss in a rotating frame. The deepening rate was found to be function of the Coriolis parameter and the stratification with the time dependency $h(t) \sim t^{1/5}$
We have showed that the turbulent kinetic energy reach a steady state after 0.5 T_f. Thus the constant input of energy by wind stress on the surface is converted to buoyancy production in a layer at the interface between the well-mixed layer above and the stratified one at rest bellow. This interface is defined by its marginal stability and concentrate most of the mixing. Therefore we shown the vertical inhomogeneity of the mixing efficiency within the mixed layer.

All the processes cited here have been studied in the context of wind-driven convection without heat flux. The extension of this work would be to study the case of free convection subject to rotation, in particular to investigate the creation of inertial waves in the absence of mean current and wind forcing . Current explanations are based either on the Taylor Proudman theorem or on the interaction of coherent vortex structures. There remains much to explore on this question.

Acknowledgments
This work has been funded by the IRGA grant 2023, distributed for the laboratory from the university of Grenoble Alpes, and the grant ANR PLUME.
The authors declare that they have no conflict of interest.

References

Burchard, H. (2002a). *Applied Turbulence Modelling in Marine Waters*. Springer Science & Business Media.
Burchard, H. (2002b). Energy-conserving discretisation of turbulent shear and

buoyancy production. *Ocean Modelling*, *4*(3), 347–361. doi: 10.1016/S1463-5003(02)00009-4

Burchard, H., & Bolding, K. (2001). Comparative Analysis of Four Second-Moment Turbulence Closure Models for the Oceanic Mixed Layer. *Journal of Physical Oceanography*, *31*(8), 1943–1968. doi: 10.1175/1520-0485(2001)031⟨1943:CAOFSM⟩2.0.CO;2

Canuto, V. M., Howard, A., Cheng, Y., & Dubovikov, M. S. (2001). Ocean Turbulence. Part I: One-Point Closure Model—Momentum and Heat Vertical Diffusivities. *Journal of Physical Oceanography*, *31*(6), 1413–1426. doi: 10.1175/1520-0485(2001)031⟨1413:OTPIOP⟩2.0.CO;2

Carpenter, J. R., Liang, Y., Timmermans, M.-L., & Heifetz, E. (2022). Physical mechanisms of the linear stabilization of convection by rotation. *Physical Review Fluids*, *7*(8), 083501. doi: 10.1103/PhysRevFluids.7.083501

Chandrasekhar, S. (1997). The instability of a layer of fluid heated below and subject to Coriolis forces. *Proceedings of the Royal Society of London. Series A. Mathematical and Physical Sciences*, *217*(1130), 306–327. doi: 10.1098/rspa.1953.0065

Fernando, H. J. S., Chen, R.-R., & Boyer, D. L. (1991). Effects of rotation on convective turbulence. *Journal of Fluid Mechanics*, *228*, 513–547. doi: 10.1017/S002211209100280X

Jones, H., & Marshall, J. (1993). Convection with Rotation in a Neutral Ocean: A Study of Open-Ocean Deep Convection. *Journal of Physical Oceanography*, *23*(6), 1009–1039. doi: 10.1175/1520-0485(1993)023⟨1009:CWRIAN⟩2.0.CO;2

Kato, H., & Phillips, O. M. (1969). On the penetration of a turbulent layer into stratified fluid. *Journal of Fluid Mechanics*, *37*(4), 643–655. doi: 10.1017/S0022112069000784

Lozovatsky, I., Figueroa, M., Roget, E., Fernando, H. J. S., & Shapovalov, S. (2005). Observations and scaling of the upper mixed layer in the North Atlantic. *Journal of Geophysical Research: Oceans*, *110*(C5). doi: 10.1029/2004JC002708

Mironov, D. V., Gryanik, V. M., Moeng, C.-H., Olbers, D. J., & Warncke, T. H. (2000). Vertical turbulence structure and second-moment budgets in convection with rotation: A large-eddy simulation study. *Quarterly Journal of the Royal Meteorological Society*, *126*(563), 477–515. doi: 10.1002/qj.49712656306

Osborn, T. R. (1980). Estimates of the Local Rate of Vertical Diffusion from Dissipation Measurements. *Journal of Physical Oceanography*, *10*(1), 83–89. doi: 10.1175/1520-0485(1980)010⟨0083:EOTLRO⟩2.0.CO;2

Pollard, R. T., Rhines, P. B., & Thompson, R. (1973). The deepening of the wind-Mixed layer. *Geophysical Fluid Dynamics*. doi: 10.1080/03091927208236105

Price, J. F., Weller, R. A., & Pinkel, R. (1986). Diurnal cycling: Observations and models of the upper ocean response to diurnal heating, cooling, and wind mixing. *Journal of Geophysical Research: Oceans*, *91*(C7), 8411–8427. doi: 10.1029/JC091iC07p08411

Rodi, W. (1987). Examples of calculation methods for flow and mixing in stratified fluids. *Journal of Geophysical Research: Oceans*, *92*(C5), 5305–5328. doi: 10.1029/JC092iC05p05305

Sander, J., Wolf-Gladrow, D., & Olbers, D. (1995). Numerical studies of open ocean deep convection. *Journal of Geophysical Research: Oceans*, *100*(C10), 20579–20600. doi: 10.1029/95JC02405

Umlauf, L., Burchard, H., & Hutter, K. (2003). Extending the k-omega turbulence model towards oceanic applications. *Ocean Modelling*, *5*(3), 195–218. doi: 10.1016/S1463-5003(02)00039-2

Ushijima, Y., & Yoshikawa, Y. (2020). Mixed layer deepening due to wind-induced shear-driven turbulence and scaling of the deepening rate in the stratified ocean. *Ocean Dynamics*, *70*(4), 505–512. doi: 10.1007/s10236-020-01344-w

Veronis, G. (1959). Cellular convection with finite amplitude in a rotating fluid. *Journal of Fluid Mechanics*, *5*(3), 401–435. doi: 10.1017/S0022112059000283

Zilitinkevich, S., Chalikov, D., & Resnyansky, Y. (1979). Modeling the oceanic upper layer. *Oceanologica Acta*.